Magnetically-actuated mesoporous nanowires for enhanced heterogeneous catalysis

Albert Serrà [a,b,*], Sergi Grau [c], Carolina Gimbert-Suriñach [c], Jordi Sort [d,e], Josep Nogués [f,e,**], Elisa Vallés [a,b,*]

[a] Grup d'Electrodeposició de Capes Primes i Nanoestructures (GE-CPN), Departament de Ciència de Materials i Química Física, Universitat de Barcelona, Martí i Franquès, 1, E-08028, Barcelona, Catalonia, Spain
[b] Institute of Nanoscience and Nanotechnology (IN²UB), Universitat de Barcelona, Spain
[c] Institute of Chemical Research of Catalonia (ICIQ), Barcelona Institute of Science and Technology, Avinguda Països Catalans 16, 43007 Tarragona, Catalonia, Spain
[d] Departament de Física, Universitat Autònoma de Barcelona, E-08193, Bellaterra, Catalonia, Spain
[e] ICREA, Pg. Lluís Companys 23, 08010, Barcelona, Spain
[f] Catalan Institute of Nanoscience and Nanotechnology (ICN2), CSIC, The Barcelona Institute of Science and Technology, Campus UAB, Bellaterra, E-08193 Barcelona, Spain

ARTICLE INFO

ABSTRACT

We study the optimization of the catalytic properties of entirely magnetic Co–Pt compact and mesoporous nanowires of different diameters (25–200 nm) by using magnetic actuation. The nanowires are a single-entity, robust, magnetic-catalyst with a huge catalytically-active surface area. We show that apart from conventional parameters, like the size and morphology of the nanowires, other factors can be optimized to enhance their catalytic activity. In particular, given the magnetic character of the nanowires, rotating magnetic fields are a very powerful approach to boost the performance of the catalyst. In particular, the magnetic field induces them to act as nano-stirrers, improving the local flow of material towards the active sites of the catalyst. We demonstrate the versatility of the procedure by optimizing (i) the degradation of different types of pollutants (4-nitrophenol and methylene blue) and (ii) hydrogen production. For example, by using as little as 0.1 mg mL^{-1} of 25 nm wide Co–Pt mesoporous nanowires (with ~3 nm pore size) as catalysts, kinetic normalized constants k_{nor} as high as 20,667 and 21,750 s^{-1} g^{-1} for 4-nitrophenol and methylene blue reduction, respectively, are obtained. In addition, activity values for hydrogen production from borohydride are as high as 25.0 L H$_2$ g^{-1} min^{-1}, even at room temperature. These values outperform any current state-of-the-art proposed catalysis strategies for water remediation reactions by at least 10-times and are superior to most advanced approaches to generate hydrogen from borohydride. The recyclability of the nanowires together with the simplicity of the synthetic method makes this approach (using not only Co–Pt, but also other mesoporous magnetic catalysts) very appealing for very diverse types of catalytic applications.

© 2017 Elsevier B.V. All rights reserved.

1. Introduction

It is well-known that catalysis plays a crucial role in our everyday life and it is one of the pillars of modern chemistry. Most industrial chemical processes (e.g., energy, pharmaceutical, food or material production industries) are based on catalytic processes [1–3]. Similarly, catalysis plays a strategic role in many environmental and energy issues such as air pollution control (e.g., car exhausts), wastewater remediation or hydrogen production [4–7]. Thus, any improvement on the performance of catalytic processes could result in a huge economic and social impact. Consequently, many different types of processes such as microwave-, plasma-, ultrasound-, electric field-, acoustic-, light- or temperature-assisted catalysis, among others, are continuously emerging as promising strategies to enhance these type of reactions [8–11]. Another aspect which is being actively explored to improve heterogeneous catalysis is to increase the surface area of

* Corresponding authors at: Grup d'Electrodeposició de Capes Primes i Nanoestructures (GE-CPN), Departament de Ciència de Materials i Química Física, Universitat de Barcelona, Martí i Franquès, 1, E-08028, Barcelona, Catalonia, Spain.
** Corresponding author at: Catalan Institute of Nanoscience and Nanotechnology (ICN2), CSIC, The Barcelona Institute of Science and Technology, Campus UAB, Bellaterra, E-08193 Barcelona, Spain.
E-mail addresses: a.serra@ub.edu (A. Serrà), josep.nogues@uab.cat (J. Nogués), e.valles@ub.edu (E. Vallés).

the catalyst, using for example nanostructured materials [12,13]. In particular, mesoporous materials, which possess an extraordinarily large specific surface area, have attracted great attention for heterogeneous catalysis in liquid media [14,15]. Additionally, of all the variables involved in heterogeneously catalysed reactions, effective mass transfer is fundamental to enhance the reaction rate, magnetic stirring bars or mechanical stirrers are usually used to promote the mass transportation efficiency [16,17]. However, delicate catalysts might be damaged under vigorous mechanical stirring or catalysts involving magnetic materials may get stuck to the magnetic stirring bars [18].

Strikingly, an aspect that has been somewhat underexploited in catalysis is magnetic actuation on the catalyst itself. In fact, during the 90 s and early 2000 s it was shown that magnetic fields could actually control the mass transport in some chemical reactions [19]. In recent years, the important role of magnetic materials in the control of magnetic field induced convection has been established [20,21]. Other attractive aspects of magnetic fields in catalysis are their influence on the oxidation process of magnetic ions or their effect on the electronic structure of the catalysts [22,23]. Although lately there has been an increase of the use of magnetic materials in catalytic processes, usually the magnetic counterpart does not play an active role in the catalysis, but it is rather used as a simple means to recover the catalyst to recycle and reuse it [24–26]. An appealing aspect of magnetic materials in catalysis, that has been proposed recently, is the concept of magnetically-actuated remote micro-stirrers [27–31]. The use of these magnetic stirrers has been shown to improve diverse types of catalytic processes by favouring the local flow of matter. However, again, in these catalysts the magnetic counterpart does not play an active role in the reaction [27–31]. Moreover, these micro-stirrers are often composites (with both magnetic and catalytic moieties and usually other components), which could make them rather fragile. Moreover, often they require complex synthesis procedures, often involving many steps, making them less attractive for large scale production [27,31].

It is important to highlight that catalysts based on magnetic ions (e.g., Fe, Co or Ni) have also started to attract a great deal of attention, although not necessarily due to their magnetic nature but due to their transition-metal character. Namely, they have been proposed as suitable candidates to partially substitute the expensive noble-metal catalysts (e.g., Pt, Au or Pd) by inexpensive alternatives, which in general improve the catalytic performance [32–35]. In particular, the partial substitution of Pt by Co has been shown to result in excellent alternatives for many different types of processes [36–39].

Here we demonstrate that easily-synthesized mesoporous Co–Pt magnetic nanowires (NWs) can be used as effective magnetically-actuated micro-stirrers to boost diverse types of catalytic reactions (e.g., for 4-nitrophenol and methylene blue degradation or hydrolysis of alkaline sodium borohydride for hydrogen production). These mesoporous NWs constitute a sturdy, *all-in-one* catalyst (i.e., a strongly catalytically active magnetic material) with a large active area, which can be easily manipulated by magnetic fields. The role of different parameters in the improved catalytic performance is investigated, such as the magnetic field rotation speed, the NW morphology and diameter and the reaction geometry. The results show that narrow mesoporous NWs magnetically actuated at high rotation speeds in planar reaction geometry is the optimum combination to achieve outstanding performances in both types of reactions. Magnetically-actuated mesoporous NWs surpass all the state-of-the-art catalysts proposed for nitrophenol and methylene blue degradation by at least a factor 10. For hydrogen production, the mesoporous NWs have similar or better performance than more complex and costly catalysts used currently.

Table 1
Electrochemical media selected for synthesising Co–Pt NWs.

Electrochemical media	W/wt.%	S/wt.%	IL/wt.%
Aqueous solution (W)	100	–	–
Ionic Liquid-in-water microemulsion (IL/W)	83.8	15.1	1.1

2. Experimental

2.1. Electrochemical media

The electrochemical media (Table 1) used for synthesising compact or mesoporous NWs were (i) an aqueous solution (W) of 2.5 mM $CoCl_2 \cdot 6H_2O$ (Carlo Erba, >98.0%) + 1.2 mM $Na_2PtCl_6 \cdot 6H_2O$ (Alfa Aesar, 98%) + 0.1 M NH_4Cl (Fluka, 99.5%) + 10 g L^{-1} H_3BO_3 (Merck, >98%) and (ii) an ionic liquid-in-water (IL/W) microemulsion, respectively. IL/W microemulsions were prepared by mixing the adequate proportion of each component [W – aqueous solution –, S – Surfactant, *p*-octyl poly (ethyleneglycol) phenyl ether a.k.a. Triton X-100 (Acros Organics, 98%) –, and IL – Ionic Liquid, 1-butyl-3-methylimidazolium hexafluorophosphate a.k.a. bmimPF$_6$ (Solvionic, 99%) –] during 5 min under magnetic stirring (300 rpm) and argon bubbling, leading to a transparent, isotropic, and thermodynamically stable microemulsion [40,41]. All solutions were prepared using deionized water (Millipore Q-System) with a resistivity of 18.2 MΩ cm.

2.2. Electrochemical synthesis

The shape-controlled electrodeposition of compact or mesoporous (double-template electrodeposition) Co–Pt NWs was carried out using a microcomputer-controlled potentiostat/galvanostat Autolab with a PGSTAT30 equipment and the GPES software. Commercial polycarbonate (PC) membranes (*Millipore Company*) with nominal pore sizes of 100 or 200 nm and alumina membranes (*SmartPor Membranes GmBH*) with a nominal pore size of 25 nm were used as working electrodes. The pores of the membranes act as templates for the shape-controlled growth of nanostructured wires, where aqueous or IL/W microemulsion media lead to either compact or mesoporous NWs. The use of microemulsions allows the formation of a three-dimensionally interconnected network of open mesopores along the entire NWs [15,40,41]. However, in order to use the membranes as a working electrode a conductive layer on one side is necessary. Therefore, vacuum evaporation was used to coat the membrane on one side with around a 100 nm-thick gold layer. The electrodeposition process was performed at 25 °C, using a three-electrode electrochemical system – polycarbonate/Alumina membranes, Pt spiral, and Ag/AgCl/KCl (3 M) electrodes, as a working, counter and reference electrodes, respectively –, in potentiostatic mode (at – 1.0 V). The electrochemical media was de-aerated by argon bubbling before each experiment and maintained under argon atmosphere during it.

After the deposition, the samples were dried and weighted several times until a constant weight in vacuum conditions was attained in order to determine the total mass of synthesized NWs. Then, the NWs were released from the membrane first removing the Au layer using a saturated solution of I_2/I^- and subsequently dissolving polycarbonate or alumina membrane with either chloroform (x10) or NaOH (1 M), and then washing with ethanol (x5) and water (x5) under flashing ultrasound stirring.

2.3. Materials characterization

The morphology of the Co–Pt NWs was examined by using transmission electron microscopy (Jeol 2100) and the elemental

composition was determined by energy-dispersive X-ray analysis incorporated in a JSM–7100 scanning electron microscopy.

Hysteresis loops of the compact and mesoporous NWs (while still embedded in the membrane) were measured at room temperature using a vibrating sample magnetometer from Micro-Sense (LOT-Quantum Design), with a maximum external magnetic field of 20 kOe, applied either along or perpendicular to the NWs axis.

The electrochemical surface area (ECSA) values of the Co–Pt NWs were determined by using cyclic voltammetries in 0.5 M H_2SO_4 at 20 mV s^{-1} at 25 °C. For each NW type, 5 µL of a NWs ink (0.1 mg mL^{-1}) was dropped on the surface of a glassy carbon (GC) rod (0.031 cm^2 in diameter) and dried under nitrogen. It is well known that for Pt-based nanostructures, the ECSA can be obtained from the total charge passed during hydrogen adsorption/desorption (after accounting for the double layer capacity and assuming that the charge required to oxidise a mono-layer of hydrogen on bright Pt is 210 µC cm^{-1}) by using the following equation (Eq. (1)) [25,38]:

$$ECSA = \frac{Q_{measured}}{Q_{theoretical} \cdot m_{Co-Pt}} \tag{1}$$

Where $Q_{measured}$ is the charge measured by integration of a voltammetric peak associated with an adsorption process, $Q_{theoretical}$ is the charge required for monolayer coverage of 1 cm^2 of electrode surface by the adsorbed species and m_{Co-Pt} is the mass of catalyst.

X-ray powder diffraction (XRPD) measurements were acquired with a PANalytical X'Pert Pro MPD diffractometer in the Bragg-Brentano reflection θ/2θ geometry, at 45 kV, 40 mA, and λ = 1.5406 Å (Cu K$_{α1}$). The samples were prepared by drop casting and solvent evaporation of the catalyst ink on a monocrystalline Si holder. XRPD patterns were obtained after θ/2θ scans from 20 to 120° 2θ, with a step size of 0.0172°, using a measuring time of 200 s per step. Note that the measurements were repeated several times to acquire sufficient statistics. The data were analysed using the X'Pert HighScore Plus software.

X-Ray photoemission spectroscopy (XPS) measurements were carried out in ultra-high vacuum using a PHI ESCA-550 multi-technique system (Physical Electronics), with a monochromatic x-ray source (Al K$_α$ line of 1486.6 eV energy and 350 W) placed perpendicular to the analyser axis and calibrated using the Ag3d$_{5/2}$ line with a full width at half maximum of 0.8 eV. The analysed area was a circle of 0.8 mm in diameter, and the selected resolution for the spectra was 187.85 eV of pass energy and 0.8 eV per step for the survey spectra.

2.4. Water remediation

The reduction of 4-nitrophenol and methylene blue was chosen as model reactions to test the catalytic activity of the compact and mesoporous Co–Pt NWs. In both reactions the temporal evolution of the catalytic reaction was tracked *ex-situ* by UV–visible spectroscopy in a quartz cuvette with an optical length of 1 cm using a UV-1800 Shimadzu UV–vis spectrophotometer. All of the experiments were conducted at room temperature. For these experiments, two different pollutants were selected:

(i) 4-nitrophenol: 300 µL of 4-nitrophenol (0.7 mM solution) were diluted with 1 mL of Millipore water, followed by the addition of 1 mL of freshly prepared ice-cold NaBH$_4$ solution (0.5 M), and a given amount of the prepared catalyst ink (0.1 mg mL^{-1}). As a result, the bright yellow solution gradually fades as the reaction progresses. The absorption peak intensity at 400 nm was used to quantify the temporal evolution of the 4-nitrophenol concentration.

(ii) Methylene blue: 300 µL of methylene blue (0.4 mM solution) were diluted with 1 mL of Millipore water, followed by the addition of 1 mL of freshly prepared ice-cold NaBH$_4$ solution (2.3 mM), and a given amount of the prepared catalyst ink (0.1 mg mL^{-1}). As a result, the dark blue solution gradually fades as the reaction progresses. The absorption peak intensity at 662 nm was used to quantify the temporal evolution of the concentration of methylene blue.

2.5. Optimization of the catalytic performance

Importantly, four different reaction conditions were pursued:

(i) Silent, where no specific actuation was carried out during the reduction reaction.

(ii) Magnetic actuation, where the NWs were influenced by an external rotatory magnetic field (∼400 Oe − magnetic stirrer RH digital – IKA) at various ration speeds.

(iii) Mechanical actuation, where the NWs were mechanically stirred at 100 rpm using a Metrohm 622 rod stirrer.

(iv) Magneto-mechanical actuation, where the NWs were simultaneously mechanically (100 rpm) and magnetically (100 rpm) stirred.

Moreover, the effects of the reaction geometry were also assessed:

(i) Vertical geometry, where the container used was "rectangular vertical", with a 10 × 10 × 26 mm^3 shape (see Fig. 2).

(ii) Planar geometry, where the container used was "cylindrical planar", with a π × 17^2 × 3 mm^3 shape or a microdroplet (∼0.1 mL) (see Fig. 2).

In the catalytic test, the concentrations of NaBH$_4$ in all the reactions are fixed at ∼2,380–times and ∼19–times higher that of 4-nitrophenol and methylene blue, respectively. Therefore, an excess amount of reductant NaBH$_4$ was used and, consequently, the reduction rate constant can be calculated based on pseudo-first-order kinetics. The apparent kinetic rate constant (k_{app}) is proportional to the total surface area of the catalyst, which can be estimated based on the regression of the slope from the logarithm plot (Eq. (2))

$$\left(\frac{dc_t}{dt} = -k_{app}c_t\right) \rightarrow \ln\left(\frac{c_t}{c_0}\right) = \ln\left(\frac{A_t}{A_0}\right) = -k_{app}t \tag{2}$$

Moreover, in order to quantitatively compare with other catalysts, the normalized rate constant (k_{nor}) was also determined, which is associated with the amount of catalyst, i.e., $k_{nor} = k_{app}/m_{Co-Pt}$. In some cases, the catalytic activity was evaluated by the degradation efficiency after 60 s by the relation between (A_{60}/A_0). Lastly, in the microdroplet experiments, the colour change of blue (methylene blue) or yellow (4-nitrophneol) to colourless was a direct indicator of the reaction progress, i.e., the catalytic activity.

2.6. Hydrogen production

The hydrolysis of sodium borohydride (Eq. (3)) was selected to test the catalytic activity of the compact and mesoporous Co–Pt NWs towards hydrogen generation.

$$NaBH_4 + 2H_2O \rightarrow NaBO_2 + 4H_2 \tag{3}$$
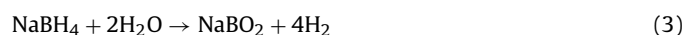
An alkaline-stabilized solution 4.2 mM sodium borohydride (adjusted to pH = 13 using NaOH 1 M), was prepared. Under these conditions, the self-hydrolysis of borohydride is minimized. Then the Co–Pt catalyst – 24 µL of a catalyst ink (0.1 mg mL^{-1}) – was used for hydrogen production in a controlled manner. The generated

hydrogen volume and the catalytic activity were measured using a Clark-type hydrogen electrode (*Unisense*) in the headspace of a gas-tight chamber containing 1 mL of total solution at 25 °C, which was calibrated with known amounts of hydrogen gas. The experimental conditions were selected to allow a quantitative comparison with previously reported results. Following the results of the catalyst optimization for water remediation (see Results section), both silent and magnetic actuation (1,200 rpm) in both vertical and planar geometry reactor conditions for compact and mesoporous Co–Pt NWs were attempted.

3. Results

3.1. Co–Pt nanowires

To evaluate the role of catalyst morphology, two types of Co-rich, $Co_{66\pm3}Pt_{34\pm3}$, NWs, 1.2 ± 0.3 μm in length and with three different diameters (25, 100 and 200 nm), were electrochemically synthesized (see Experimental) [28,38]. As can be seen in Fig. 1a, b and Table S1, for the 100 nm NWs, while one type of NW is compact (with a smooth surface), the other one has a mesoporous morphology with an interconnected network of pores (with a pore size of about 3.1 ± 0.9 nm and an extraordinary high surface area [electrochemically active surface area (ECSA)] of 255 m^2 g^{-1}– Fig. 1d and Table S1). Importantly, the elemental maps of the Co–Pt NWs (Fig. 1a, b) show that Co and Pt are homogeneously distributed along the whole NWs, both for the compact and mesoporous NWs.

Both types of NWs are magnetic at room temperature with somewhat similar magnetic characteristics, with the easy axis along the NW axis (Fig. 1c).

The crystal structure of the Co–Pt NWs was probed by using x-ray diffraction (XRPD) (Fig. 1e). From the patterns three families of peaks can be identified: *fcc* Au, corresponding to some remaining gold in the NWs from the working electrode (highlighted by dotted green arrows), *fcc* CoPt₃ (*Pm*-3m) (highlighted by dotted red arrows) and a hexagonal *hcp* Co–Pt phase (P6₃mmc) (marked by its Miller indices). Note that this latter phase corresponds to *hcp* Co but very distorted due to the incorporation of Pt atoms in the crystalline lattice. Since the patterns of compact and mesoporous NWs are almost identical, it is clear that they have analogous crystalline structures, composed of polycrystalline cubic and hcp phases. Note that similar crystalline structures have been reported for electrodeposited Co–Pt films and nanostructured materials [42,43]. The bimetallic nature of the prepared NWs is further confirmed by XPS analysis. The high-resolution scans of the XPS spectra (Fig. 1f) show for Pt double peaks with binding energies of 71.80 eV (4f₇/₂) and 75.21 eV (4f₅/₂), clearly shifted from the standard values for pure Pt (i.e., 71.20 and 74.53 eV). These values are consistent with the formation of a Co–Pt alloy since Pt 4f peaks are known to change to higher energies when alloying with Co [44]. On the other hand, for Co, two peaks at 778.7 eV (Co 2p₃/₂) and 794.0 eV (Co 2p₁/₂) are observed, which deviate from the standard values of pure Co (778.30 eV and 793.27 eV). In concordance to the Pt peaks, the shift in energy of the Co peaks is also consistent with the formation of a Co–Pt alloy [44]. Note also that although the Co 2p spectra also shows the formation of some cobalt oxides the relative intensity of the oxide peaks indicates that only a small fraction of Co is oxidized. It is important to emphasize that the XPS spectra for both types of NWs is almost identical in agreement with the EDX results.

3.2. Water remediation

3.2.1. Basic catalytic activity

Before evaluating the catalytic activity, it is important to analyse the adsorption of the two compounds on the NWs since this may interfere in the degradation process. It is well-known that some materials, particularly when nanostructured, can physically adsorb pollutants on their surface, such as 4-nitrophenol and methylene blue, as a consequence of the surface affinity [45–47]. Consequently, the absorbance of various solutions of each pollutant (<u>without</u> the presence of sodium borohydride) was measured before and after 24 and 48 h posteriorly to the addition of the NWs (either compact or mesoporous), both in silent mode or in the presence of an external rotatory magnetic field (~400 Oe and 1,200 rpm). In all cases, the absorbance remains virtually constant even after 48 h. Therefore we can conclude that the adsorption of these pollutants on the Co–Pt NWs is not significant. It is also plausible to assume that in the presence of borohydride the capture of pollutants should become even more negligible due to the formation of hydrogen bubbles on the catalyst surface and the concomitant pollutant degradation.

To test the catalytic activity, the 100 nm diameter NWs are used to degrade two different types of well-known wastewater pollutants: 4-nitrophenol and methylene blue. Both types of NWs can trigger the reduction of 4-nitrophenol and methylene blue, confirming the good catalytic properties of the Co–Pt alloys (see Fig. S1, Table S2 and Videos S1 and S2). Moreover, the mesoporous NWs are clearly more effective than the compact ones in promoting the degradation of 4-nitrophenol and methylene blue, reducing the reaction time by 4 (4-nitrophenol) or 2 (methylene blue), respectively. This is expected from the high surface area of the mesoporous wires, which exposes more active sites to carry out the reaction. In fact, the apparent kinetic constants k_{app} (and the mass normalized constant, k_{nor}) of both reactions for the mesoporous wires (i.e., without mechanical or magnetic stirring), are already rather large, k_{nor} = 3,807 s^{-1} g^{-1} (4-nitrophenol) and k_{nor} = 3,916 s^{-1} g^{-1} (methylene blue) (Table S2) and comparable with other types of catalysis proposed for these reactions (see Table S3) [27,48–56]. Importantly, the release of H_2 gas in solution by the catalysed hydrolysis of sodium borohydride (see Videos S1 and S2) implies the self-pumping of the fluid medium at the micro and nanoscale levels and, therefore, the enhancement of the mass transport flow. However, the efficiency of the reaction is somewhat restricted by the limited flow of material towards the catalyst, which is basically driven by diffusion. Thus, to favour the mass flow, the same reactions were carried out by applying mechanical stirring at 100 rpm (see Fig. S2 and Videos S1 and S2). As expected, mechanical stirring improves the reaction kinetics; nevertheless, the gain is somewhat moderate, with a 15–30% improvement in k_{nor} for the two types of reactions (see Table S2).

3.2.2. Magnetically-assisted catalysis

As a first assessment of the role of the magnetic field in the catalysis, the reduction of 4-nitrophenol and methylene blue was carried out in the presence of an out-of-plane static field of 200 Oe for the 100 nm NWs. Remarkably, the mere presence of a magnetic field already improves the efficiency of the reaction (Table S2, and Videos S3–S4), with an enhanced k_{nor} by 10–15%. This is in agreement with earlier studies in other types of catalysts where the magnetic fields (and/or field gradients generated by the magnetic catalysis or magnetic objects in close proximity to the catalytic front) enhanced the catalytic activity [31,57]. However, based on the chemical nature of both pollutants, the origin of the effect of magnetic fields on the kinetics of degradation is not straightforward. Thus, the experiments were repeated with different magnetic field intensities (i.e., 200, 110 and 45 Oe). Interestingly, the enhanced performance is roughly independent of the magnetic field. Probably, one of the effects of the field is to orient the NWs out-of-plane, thus exposing a larger effective area for the reaction. Note that, given the moderate magnetization of the wires and their light weight, the magnetic field necessary to exert sufficient toque ($\tau = \mathbf{m} \times \mathbf{H}$, where
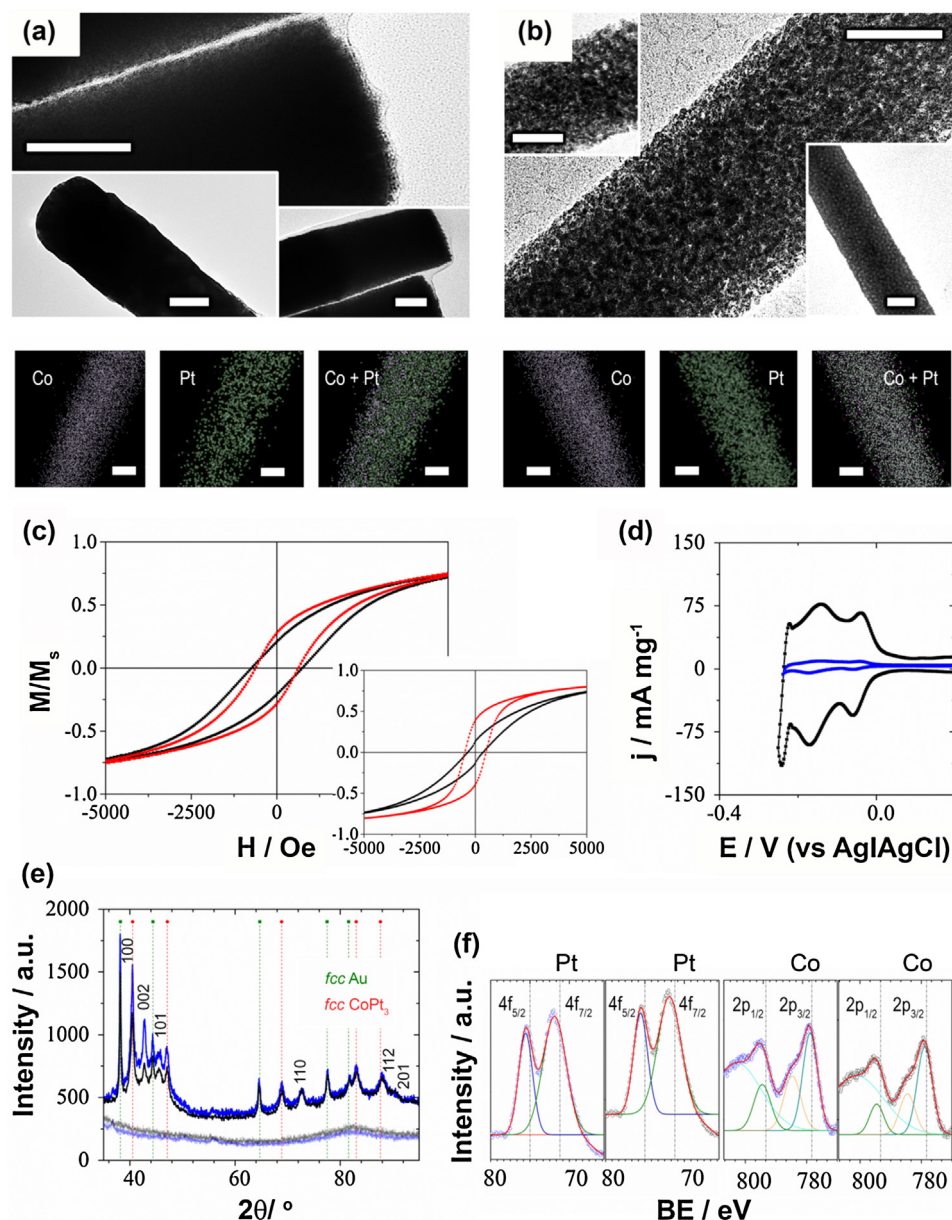
Fig. 1. HR-TEM images and elemental mapping of (a) compact and (b) mesoporous 100 nm NWs. Scale bar 50 nm. (c) Room-temperature parallel (red) and perpendicular (black) to the wire axis hysteresis loop of mesoporous 100 nm NWs (inset: compact NWs). (d) Cyclic voltammetries of the compact (blue) and mesoporous (black) NWs. (e) XRD patterns of compact (blue) and mesoporous (black) NWs. The Miller indexes of the main peaks of the hexagonal Co–Pt phase are indicated next to the corresponding peaks. The fcc Au and fcc CoPt$_3$ phases are highlighted by green and red dotted arrows, respectively. At the bottom, the Si holder background for each sample is also shown. (f) Pt 4f and Co 2p XPS spectra from the compact (blue) and mesoporous (black) NWs. (For interpretation of the references to colour in this figure legend, the reader is referred to the web version of this article.)

m is the magnetic moment and **H** the applied field) to rotate them should probably be quite small. In addition, due to the nanometric morphology of the mesoporous wires, with multiple edges, field gradients should presumably be large even for relatively small applied fields [20,21].

To asses a second aspect of the magnetic field actuation, the reactions were performed using a rotating magnetic field (400 Oe) at different speeds. Note that the experiment was carried out using a magnetic stirring set up; however, no macroscopic magnetic bar was introduced in the container. Instead, the magnetic NWs themselves act as micro-stirring bars by the effect of the rotating field (see Fig. 2). As can be seen in Fig. 3 (and Figs. S3–S9, Table S2 and Videos S1 and S2), the rotating magnetic field has an outstanding effect on the effectiveness of the reaction, drastically reducing the reaction time to degrade 4-nitrophenol and methylene blue.

Importantly, the effect of the field increases for higher rotating speeds. For example, the time for a full degradation of 4-nitrophenol and methylene blue is reduced by an excellent 2-fold factor when comparing the experiment in absence of magnetic field with that in which a 1,200 rpm rotating field is applied. In fact, the k_{nor} values for the mesoporous NWs for both types of reactions (Fig. 3a and Table S2) are exceptionally high, outperforming all state-of-the-art catalysts proposed to date to degrade these pollutants (see Table S4). It is likely that the local magnetic field (and field gradients) promote a better local circulation of the liquid containing the pollutant, allowing it to easily reach the catalyst. However, as can be seen in the evolution of k_{nor} with rotating speed (Fig. 3) there is a tendency towards saturation for the highest speeds. This is probably caused by the fact that for sufficiently high speeds the NWs will no longer be able to follow the field. If fact, for even higher
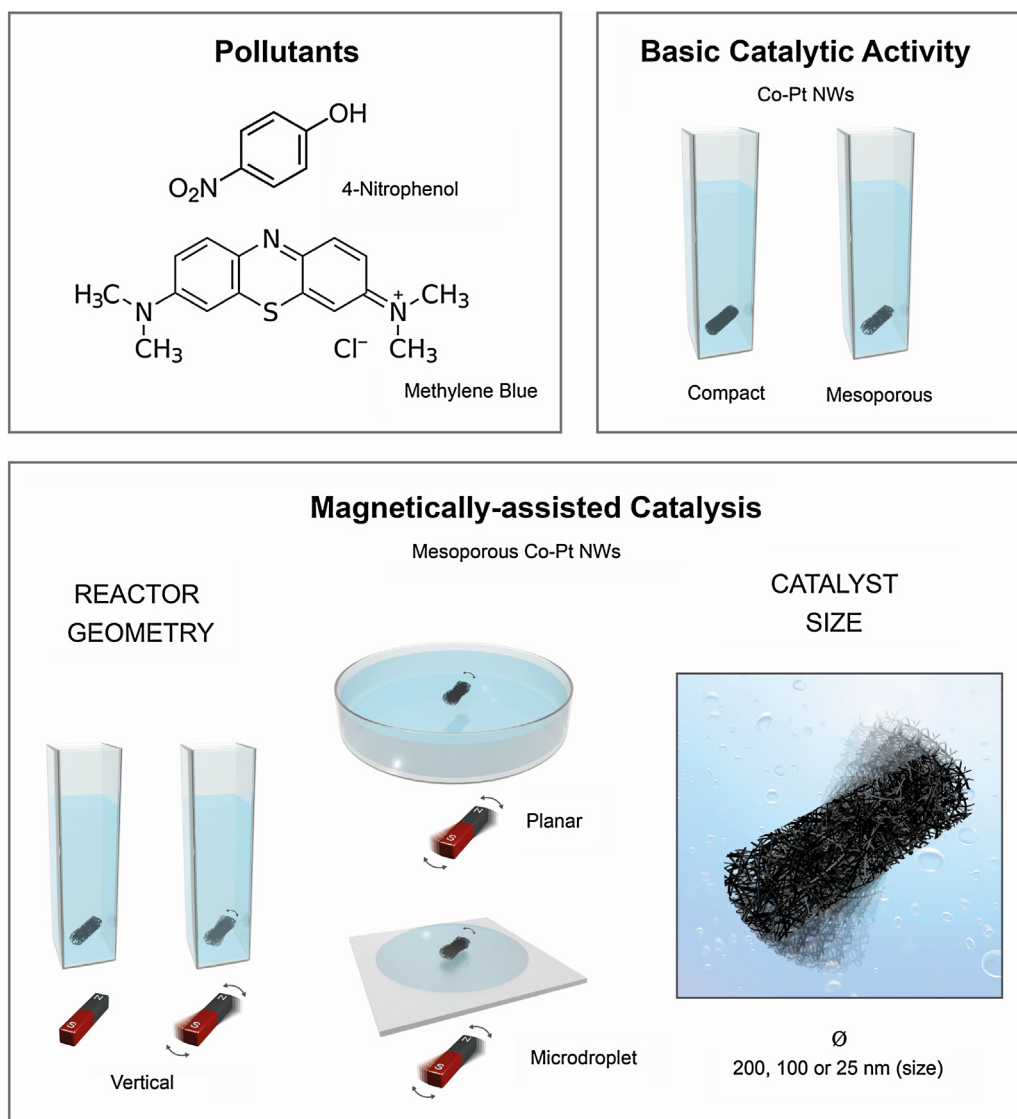
Fig. 2. Scheme of the different reaction conditions.

speeds other effects, like the heating of the wires due to hysteresis losses, could lead to new consequences in the reaction [31,57].

The experiment was repeated with a different magnetic stirrer with a smaller magnetic field (180, 80 Oe at 1,200 rpm). Interestingly, the results are virtually the same for the three fields tested (see Table S4), where the small differences probably arise from the slightly different field profiles form each device. This indicates that if the magnetic field has sufficient strength to efficiently rotate the wires (i.e., to overcome the fluid drag), its magnitude is not critical. However, eventually, if the field becomes exceedingly small it will no longer be able to rotate the NWs and consequently the enhanced performance should be lost.

In an attempt to further enhance the catalytic activity, magnetic and mechanical stirring were combined. The experiment was carried out using mechanical stirring at 100 rpm together with a rotating magnetic field at the same frequency (Fig. S7 and Videos S1 and S2). However, surprisingly, although the combined approach resulted in a better performance than mechanical stirring alone, it was worse than pure magnetic stirring. This probably stems from the fact that mechanical stirring not only displaces the liquid but also the catalyst NWs. As the NWs are moved away from the bottom of the container by the mechanical stirring, the magnetic field they

feel becomes considerably weaker (the field decreases roughly as $1/d^3$, where d is the distance), thus the advantageous effects of the magnetic field (local stirring and magnetic field gradient effects) are progressively lost.

In a more classical role of catalysts with magnetic materials, the recyclability of the NW catalysts was also evaluated. As can be seen in Figs. S10 and S11, both compact and mesoporous NWs showed excellent stability during cycling tests, where no obvious decrease of activity even after eight cycles was observed.

3.2.3. Role of the reaction geometry

The above experiments evidence the importance of the mass flow to improve the time needed to fully degrade the 4-nitrophenol and methylene blue pollutants. Moreover, it is clear that the optimum performance of the NWs is attained when they are close to the magnet. Thus, for an additional optimization of the magnetic actuation in the catalytic reaction, the role of the shape of the reaction vessel from vertical to planar geometry was evaluated using the 100 nm diameter wires. Two types of approaches were investigated (Fig. 2): (i) microdroplets and (ii) a wide container with low height (with the same reaction volume as the vertical case). The former experiment is important for lab-in-a-chip and microfluidics
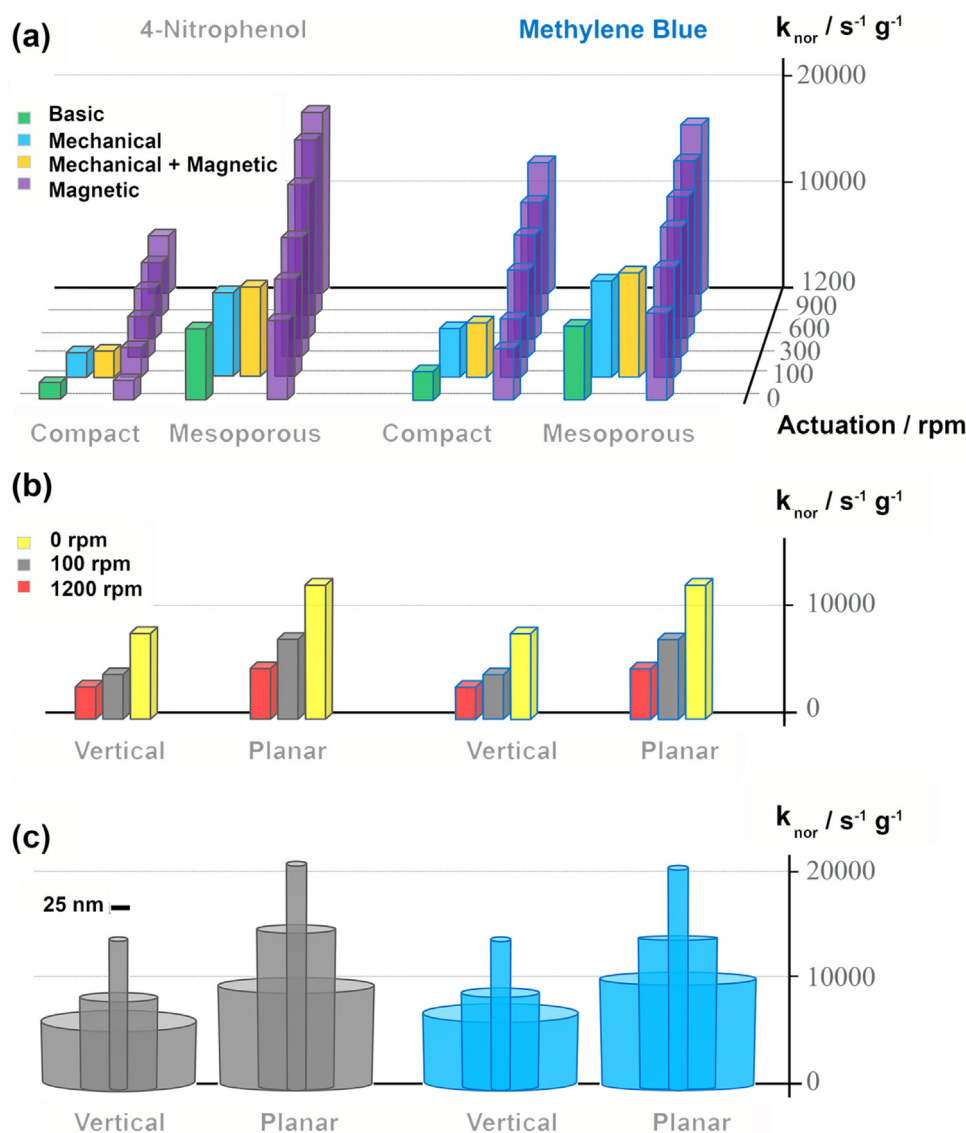
Fig. 3. Values of the normalized rate constants, k_{nor}, for the pollutants degradation. (a) Actuation type for Co–Pt 100 nm NWs. (b) Influence of the reactor geometry for Co–Pt 100 nm NWs at different magnetic actuation (c) Influence of the catalyst diameter of Co–Pt NWs (200, 100 and 25 nm) at 1,200 rpm of magnetic actuation.

type of applications, while the latter would be more relevant for large-scale applications like waterwaste remediation.

Due to their small size, the quantitative evolution of the reaction in the microdroplets is rather complex. Thus, to evaluate the performance of the mesoporous NWs in the microdroplets, the discoloration in the different configurations was compared (see Videos S5 and S6). Indeed, the degradation of 4-nitrophenol and methylene blue proceeds considerably faster in the microdroplets than in the conventional container under the same magnetic field conditions. This is in concordance with the results obtained with composite microstirrers, which were shown to efficiently enhance the catalysis of diverse types of reactions in microdroplet conditions [16,17].

Similar effects are obtained when the experiment is carried out in a macroscopic container. Remarkably, just by changing the geometry of the reaction container from "rectangular vertical" to "cylindrical planar" geometry (see Fig. 2) and maintaining the same reaction volume and the same magnetic stirring conditions (100 rpm and 1,200 rpm), the efficiency of the reactions almost doubles leading to k_{nor} as high as 14,058 $s^{-1} g^{-1}$ and 14,600 $s^{-1} g^{-1}$ for 4-nitrophenol and methylene blue, respectively (see Figs. 3b, S12, Table S5 and Videos S7 and S8). These results clearly highlight the

importance of the geometry to optimize the role of the magnetic field.

3.2.4. Role of the catalyst size

In a final attempt to further optimize the efficiency of the catalytic reactions we investigate the effect of the diameter of the mesoporous Co–Pt NWs. The idea of using different diameters is two-fold: (i) to assess the effect that the geometry of the NWs may have in the microstirring process and (ii) to evaluate the role of the surface area of the NWs, which increases as the diameter is decreased (Table S5).

The degradation of the water pollutants was carried out at 1,200 rpm both in vertical and planar containers. The results, shown in Fig. 3c, Table S5 and Fig. S13, unambiguously demonstrate that in all the conditions the narrower 25 nm wires have a significantly better performance for both types of reactions than the wider ones. The best performance is obtained for mesoporous 25 nm NWs at 1,200 rpm in planar geometry, with k_{nor} = 20,667 and 21,750 $s^{-1} g^{-1}$, for 4-nitrophenol and methylene blue, respectively.

Interestingly, when comparing the increase in surface area with the enhanced catalytic performance it is clear that apart from the
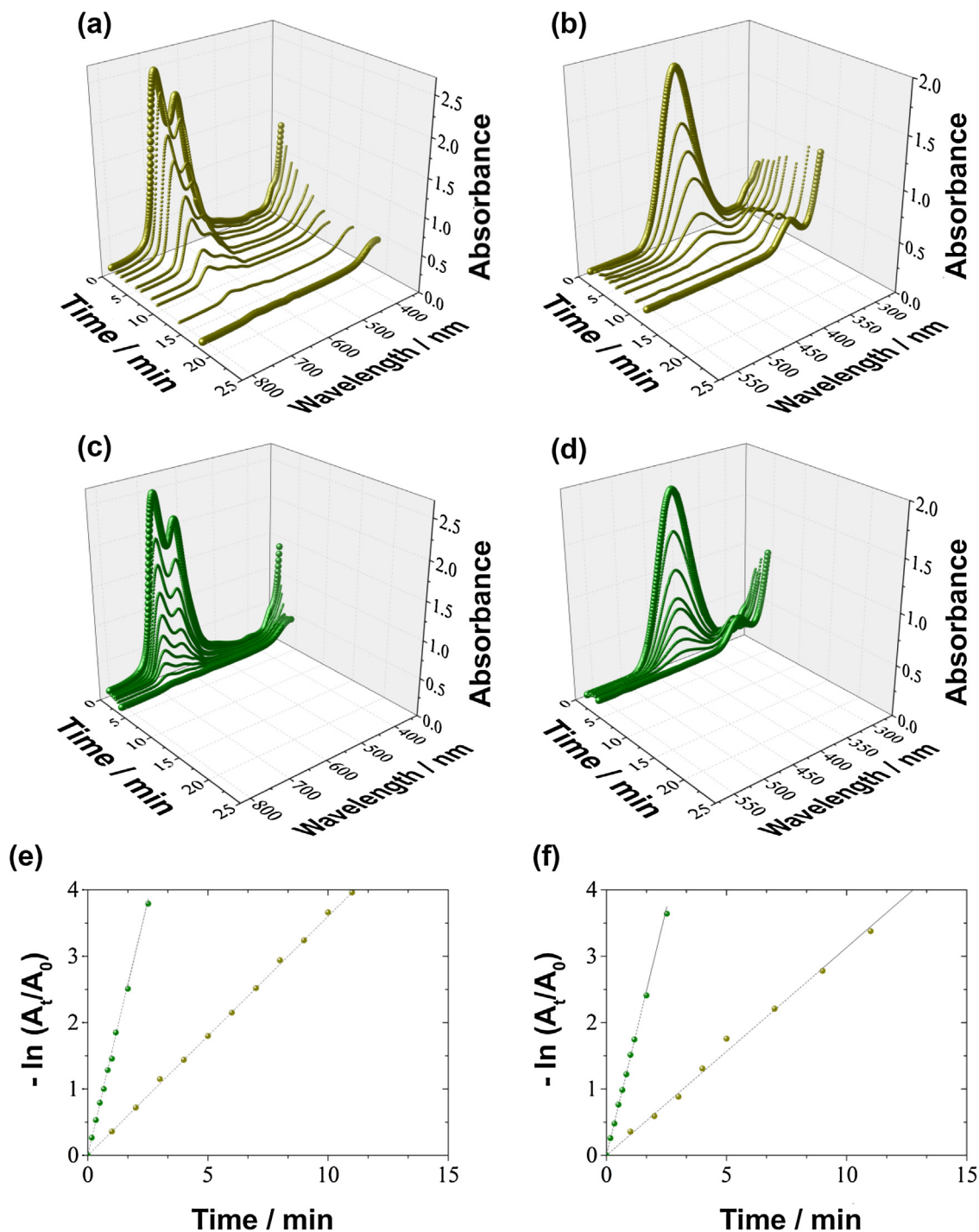
Fig. 4. Time-dependent UV–visible spectra of 4-nitrophenol (a, c) and methylene blue (b, d) catalysed reduction in (dark yellow) mechanical actuation (catalyst diameter: 100 nm; actuation: 100 rpm; geometry: vertical) and (green) magnetic actuation (catalyst diameter: 100 nm; actuation: 1,200 rpm; geometry: planar) conditions, in which 12 μL of a suspension of mesoporous Co–Pt NWs (0.1 mg mL^{-1}) were added. Plots of $-\ln(A_t/A_0)$ against reaction time for the catalyzed reduction of (e) 4-nitrophenol or (f) methylene blue under (dark yellow) mechanical actuation (catalyst diameter: 100 nm; actuation: 100 rpm; geometry: vertical) and (green) magnetic actuation (catalyst diameter: 100 nm; actuation: 1,200 rpm; geometry: planar) conditions, in which 12 μL of a suspension of mesoporous Co–Pt NWs (0.1 mg mL^{-1}) were added. (For interpretation of the references to colour in this figure legend, the reader is referred to the web version of this article.)

surface area, the magnetic actuation also plays an important role in the catalytic activity. Namely, when decreasing the diameter from 200 nm to 25 nm, the surface area only increases a factor ECSA(25 nm)/ECSA(200 nm) = 1.56, while the kinetic constant improves substantially more $k_{nor}(25\,nm)/k_{nor}(200\,nm) = 2.2$.

Remarkably, when comparing the somewhat standard procedure of 100 nm compact NWs with mechanical stirring in a vertical container with the novel approach of 25 nm mesoporous NWs with 1,200 rpm magnetic microstirring in a planar container the gain in efficiency is simply impressive, reducing the degradation time by a factor 5.5 (Fig. 4). This results in an improved mass normalized apparent kinetic constant of $k_{nor} = 20,667$ and $21,750\,s^{-1}\,g^{-1}$, which considerably exceeds all standard and advanced procedures for 4-nitrophenol and methylene blue degradation.

3.3. Hydrogen production

It is well known that sodium borohydride ($NaBH_4$) is a pre-eminent candidate for pure hydrogen generation by means of its irreversible hydrolysis (Eq. (3)), with the significant advantage that 50% of the produced hydrogen originates from water itself, since sodium borohydride is a water-splitting agent [58–61]. Importantly, the formation of hydrogen from borohydride decomposition produces pure H_2 without carbon contaminations such as CO or CO_2. Moreover, $NaBH_4$ is stable, non-flammable, non-toxic and it is able to store hydrogen with a capacity of 10.8 wt.%. [61–63]. Sodium metaborate ($NaBO_2$), which is formed simultaneously to hydrogen in the reaction described in Eq. (3), is also environmentally clean and it can actually be recycled by electrosynthesizing it back to sodium borohydride (Eq. (4)) [58]:

$$NaBO_2 + 2H_2O \rightarrow NaBH_4 + 2O_2 \qquad (4)$$

Hence, in these conditions, only water would be consumed for hydrogen production. Consequently, borohydride is a great candidate for direct fuel cells [64–66]. By extension, the development of competitive catalysts for this type of reaction is of major importance; especially using catalysts viable for industrial applications (i.e. low cost and good catalytic activity), since the non-catalysed hydrolysis is extremely slow (see Fig. S14).

The magnetically-actuated catalysis for hydrogen production was determined by measuring the hydrogen generation yield as a function of time in both vertical ($\pi \times 7^2 \times 7.0\,mm^3$) and planar ($\pi \times 12^2 \times 2.4\,mm^3$) reaction conditions using compact and mesoporous 25 nm NWs. Figs. 5 and S15 and Table 2 show that the catalytic performance dramatically depends on three factors: (i) catalyst nature; (ii) reactor geometry; and (iii) use or not of magnetic actuation. In agreement with the pollutant degradation reactions the combination of mesoporosity, planar geometry and magnetic actuation renders the best hydrogen generation activity, leading to remarkable 25.0 L H_2 g^{-1} min^{-1}. In fact, in these conditions the reaction reaches its maximum yield in less than 1,000 s (Figs. 5 and S15 and Table 2). Hence, the three factors together play a synergetic role in optimizing the kinetics of heterogeneous catalysis. For example, compared to the reaction using magnetically actuated compact NWs in vertical geometry, an impressive 312 x improvement is obtained (compare entries i and vi in Table 2). Importantly, the maximum values of hydrogen generation rate were obtained by a differential procedure and correspond to the instantaneous rate at t = 0 s. However, these values do not necessarily match exactly the maximum reaction rate for mesoporous NWs as a consequence of the pore diffusion resistance [66,67]. Despite this limitation, the values for the hydrogen generation activity are far better than in many other catalysts and are actually comparable to the more competitive state-of-the-art solid catalysts based on noble metals [31,58–74] (Table S6). In addition,
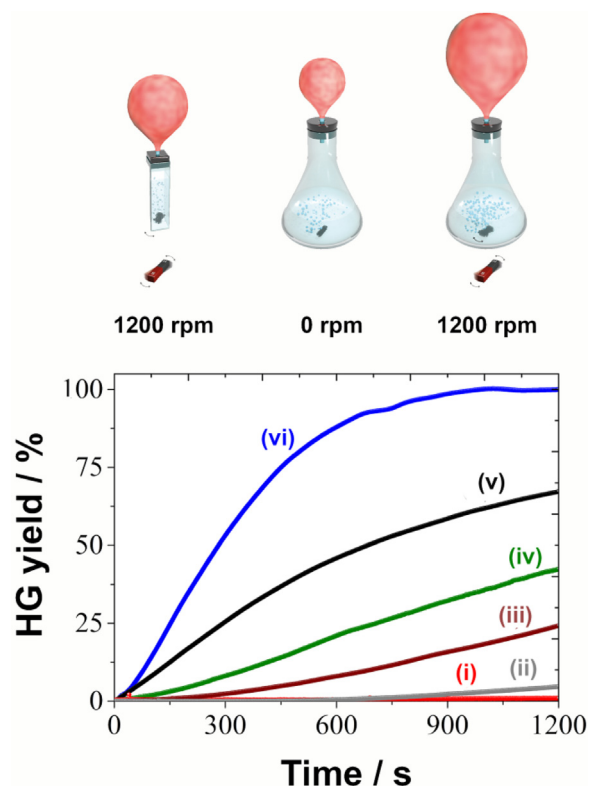

Fig. 5. Hydrogen generation (HG) yield as a function of reaction time for compact (i, ii, iii) mesoporous (iv, v, vi) 25 nm NWs in planar (ii, iii, v, vi) or vertical (i, iv) reaction geometry and silent (ii and v) or magnetic actuation (i, iii, iv, and vi) conditions.

this approach offers the relevant advantage of reducing the Pt content (i.e., cost-effectiveness) and the important benefits from the magnetic behaviour of the catalysts, i.e., easy manipulation, recyclability and improved catalytic performance. Nevertheless, it should be emphasized that the hydrogen generation activity values in Table 2 are based on the use of *only* 4.2 mM of $NaBH_4$, while most of the reactions reported in Table S6 use between 50 and 1,000 times more $NaBH_4$. Since the hydrolysis of $NaBH_4$ cannot be clearly considered as a zero-order reaction [75,76], the catalytic activity should depend on the amount of $NaBH_4$. Taking this fact into account, using magnetically actuated mesoporous Co–Pt NWs in planar geometry should far surpass all current hydrogen generation approaches based on $NaBH_4$.

Table 2

Comparison of catalytic conditions and hydrogen generation performance of compact and mesoporous 25 nm NWs in vertical and planar reaction geometry and silent and magnetic actuated heterogeneous catalysis. All reactions were performed using 1 mL of 4.2 mM $NaBH_4$ (pH 13) and 24 µL of a catalyst ink (0.1 mg mL^{-1}) at 25 °C.

Entry	Catalyst	Reactor geometry	Magnetic Actuation/rpm	Hydrogen generation yield (1,200 s)/%	Activity/L H_2 g_{cat}^{-1} min^{-1}	Activity Enhancement[a]
i	Compact NWs	Vertical	1,200	1.0	0.08	1
ii	Compact NWs	Planar	0	4.6	0.25	3.1
iii	Compact NWs	Planar	1,200	24.1	1.50	18.8
iv	Mesoporous NWs	Vertical	1,200	41.8	3.02	37.8
v	Mesoporous NWs	Planar	0	67.2	10.00	125
vi	Mesoporous NWs	Planar	1,200	100.0	25.00	312.5

[a] Relative to experiment i.

4. Conclusions

Summarizing, we have evaluated magnetic actuation of entirely magnetic NWs as a novel procedure to enhance the catalytic activity for two significant reactions in the environmental and energy fields: the reduction reaction of 4-nitrophenol and methylene blue water pollutants with borohydride and pure-hydrogen production by means of borohydride decomposition. These NWs have a huge catalytically active surface and are easily manipulated (i.e., remote stirring) using magnetic fields, combined in a simple, inexpensive, single material (in contrast to most previous multicomponent complex advanced magnetic catalysts). The results show that there are several aspects which need to be adjusted for optimal performance: (i) mesoporous NWs are much more effective than compact ones; (ii) high-speed (1,200 rpm) magnetic actuation is shown to be far more effective than mechanical stirring in speeding the degradation process; (iii) planar geometry is better than vertical one; and (iv) narrow NWs (25 nm) evidence a considerably better catalytic performance than wider ones (200 nm). In fact, 25 nm mesoporous NWs with 1,200 rpm magnetic microstirring in a planar container have an excellent degradation activity with $k_{nor} = 20,667$ and $21,750 \, s^{-1} \, g^{-1}$, for 4-nitrophenol and methylene blue, respectively, and a very effective room temperature rate constant of $25.0 \, L \, H_2 \, g^{-1} \, min^{-1}$ for hydrogen production. These outstanding performances demonstrate that *magnetic actuation* (magnetic field induced convection and remote magnetic microstirring) of *purely magnetic narrow mesoporous NWs* is an efficient way to greatly enhance the catalytic efficiency in different reactions of heterogeneous catalysis, including energy production by fuel cells. Interestingly, the advantages of using Co–Pt mesoporous NWs as an entirely magnetic catalyst are numerous: (i) it results in magnetic field-induced convection, (ii) it can be used as a remote microstirring device, (iii) it allows easy and efficient recyclability, (iv) it is very robust, (v) it benefits from a cost-effective and easily scalable synthesis that does not require of hybrid multicomponent catalysts and (vi) it reduces the cost of materials since the amount of Pt precious metal is reduced. Hence, the high efficiency of magnetic actuation together with the simplicity and cost-effective synthesis approach and the efficient recyclability of the magnetic mesoporous NW catalysts make this approach very appealing to commercialize new viable alternatives for ecological decontamination and clean energy production.

Acknowledgements

Appendix A. Supplementary data

Supplementary data associated with this article can be found, in the online version, at http://dx.doi.org/10.1016/j.apcatb.2017.05.071

References

[1] S. Hu, M.R. Shaner, J.A. Beardslee, M. Lichterman, B.S. Brunschwig, N.S. Lewis, Amorphous TiO₂ coatings stabilize Si, GaAs, and GaP photoanodes for efficient water oxidation, Science 344 (2014) 1005–1009.

[2] S. Bag, A.F. Gaudette, M.E. Bussell, M.G. Kanatzidis, Spongy chalcogels of non-platinum metals act as effective hydrodesulfurization catalysts, Nat. Chem. 1 (2009) 217–224.

[3] J.K. Nørskov, T. Bligaard, J. Rossmeis, C.H. Christensen, Towards the computational design of solid catalysts, Nat. Chem. 1 (2009) 37–46.

[4] F. Nakajima, Air pollution control with catalysis –past present and future –, Catal. Today 10 (1991) 1–20.

[5] P.A. Pekakis, N.P. Xekoukoulotakis, D. Mantzavinos, Treatment of textile dyehouse wastewater by TiO₂ photocatalysis, Water Res. 40 (2006) 1276–1286.

[6] F. Mushtag, M. Guerrero, M. Selmon-Sakar, M. Hoop, A. Lindo, J. Sort, X. Chen, B.J. Nelson, E. Pellicer, S. Pané, Magnetically driven Bi₂O₃/BiOCl⁻ based hybrid microrobots for photocatalytic water remediation, J. Mater. Chem. A 3 (2015) 23670–23683.

[7] I. Galvano-Escobal, S. Suriñach, M.D. Baró, S. Pané, J. Sort, E. Pellicer, Electrodeposition of sizeable and compositionally tunable rhodium-iron nanoparticles and their activity toward hydrogen evolution reaction, Electrochim. Acta 194 (2016) 263–275.

[8] A.C. Aragonès, N.L. Haworth, N. Darwish, S. Ciampi, N.J. Bloomfield, G.G. Wallace, I. Diez-Perez, M.L. Coote, Electrostatic catalysis of a Diels-Alder reaction, Nature 531 (2016) 88–91.

[9] J.-T. Li, J.-F. Han, J.-H. Yang, T.-S. Li, An efficient synthesis of 3, 4-dihydropyrimidin-2-ones catalysed by NH₂SO₃H under ultrasound irradiation, Ultrason. Sonochem. 10 (2003) 119–122.

[10] X. Chen, L. Liu, P.Y. Yu, S.S. Mao, Increasing solar absorption for photocatalysis with black hydrogenated titanium dioxide nanocrystals, Science 331 (2011) 746–750.

[11] T. Noël, J.R. Naber, R.L. Hartman, J.P. McMullen, K.F. Jensen, S.L. Buchwald, Palladium-catalyzed amination reactions in flow: overcoming the challenges of clogging via acoustic irradiation, Chem. Sci. 2 (2011) 287–290.

[12] D. Astruc, F. Lu, J.R. Aranzaes, Nanoparticles as recyclable catalysts: the frontier between homogeneous and heterogeneous catalysis, Angew. Chem. Int. Ed. 44 (2005) 7852–7872.

[13] B. Hinnemann, P.G. Moses, J. Bonde, K.P. Jorgensen, J.H. Nielsen, S. Horch, I. Chorkendorff, J.K. Norskov, Biomimetic hydrogen evolution: MoS₂ nanoparticles as catalyst for hydrogen evolution, J. Am. Chem. Soc. 127 (2005) 5308–5309.

[14] A. Taguchi, F. Schüth, Ordered mesoporous materials in catalysis, Micropor. Mesopor. Mater. 77 (2005) 1–45.

[15] A. Serrà, E. Gómez, E. Vallés, Novel electrodeposition media to synthesize CoNi-Pt core@shell stable mesoporous nanorods with very high active surface for methanol electro-oxidation, Electrochim. Acta 174 (2015) 630–639.

[16] S. Yang, C. Cao, Y. Sun, P. Huang, F. Wei, S. Weiguo, Nanoscale magnetic stirrers bar for heterogeneous catalysis in microscopic systems, Angew. Chem. Int. Ed. 54 (2015) 2661–2664.

[17] S.L. Biswal, A.P. Gast, Micromixing with linked chains of paramagnetic particles, Anal. Chem. 76 (2004) 6648–6655.

[18] I. Petosuis, E. Homburg, R. Derks, A. Dietzel, Transient behaviour of magnetic micro-bead chains rotating in a fluid by external, Lab. Chip 7 (2007) 1746–1751.

[19] G. Hinds, J.M.D. Coey, M.E.G. Lyons, Influence of magnetic forces on electrochemical mass transport, Electrochem. Commun. 3 (2011) 215–218.

[20] L.M.A. Monzon, J.M.D. Coey, Magnetic fields in electrochemistry: the Lorentz force. A mini-review, Electrochem. Commun. 42 (2014) 38–41.

[21] L.M.A. Monzon, L.M.A. Coey, Magnetic fields in electrochemistry: the Kelvin force. A mini-review, Electrochem. Commun. 42 (2014) 42–45.

[22] X. Xiong, Y. Sun, B. Sun, W. Song, J. Sun, N. Gao, J. Qiao, X. Guan, Enhancement of the advanced Fenton process by weak magnetic field for the degradation of 4-nitrophenol, RSC Adv. 5 (2015) 13357–13365.

[23] J. Sá, J. Szlachetko, M. Sikora, M. Kavcic, O.V. Safonovam, M. Nachtegaal, Magnetic manipulation of molecules on non-magnetic catalytic surface, Nanoscale 5 (2013) 8462–8465.

[24] D. Wang, D. Astruc, Fast-growing field of magnetically recyclable nanocatalysts, Chem. Rev. 114 (2014) 6949–6985.

[25] A. Serrà, E. Gómez, E. Vallés, Facile electrochemical synthesisusing microemulsions with ionic liquid, of highly mesoporous CoPt nanorods with enhanced electrocatalytic performance for clean energy, Int. J. Hydrogen Energy 40 (2015) 8062–8070.

[26] J. Xia, Y. Fu, G. He, X. Sun, X. Wang, Core-shell-like Ni-Pd nanoparticles supported on carbon black as a magnetically separable catalyst for green Suzuki-Miyaura coupling reactions, Appl. Catal. B: Environ. 200 (2017) 39–46.

[27] S.K. Srivastava, M. Guix, O.G. Schmidt, Wastewater mediated activation of Micromotors for efficient water cleaning, Nano Lett. 16 (2015) 817–821.

[28] D. Vilela, J. Parmar, Y. Zeng, Y. Zhao, S. Sánchez, Graphene-based microrobots for toxic heavy metal removal and recovery from water, Nano Lett. 16 (2015) 2860–2866.

[29] W.H. Chong, L.K. Chin, R.L. Tan, H. Wang, A.Q. Liu, H. Chen, Stirring in suspension: nanometer-sized magnetic stir bars, Angew. Chem. Ed. Int. 52 (2013) 8570–8573.

[30] S. Yang, C. Cao, L. Peng, P. Huang, Y. Sun, F. Wei, W. Song, Spindle-shaped nanoscale yolk/shell magnetic stirring bars for heterogeneous catalysis in macro- and microscopic systems, Chem. Commun. 52 (2016) 1575–1578.

[31] Y. Liu, J. Zhang, X. Zhang, B. Li, X. Wang, H. Cao, D. Wei, Z. Zhou, A.K. Cheetham, Magnetic catalysts as nanoactuators to achieve simultaneous momentum-transfer and continuous-flow hydrogen production, J. Mater. Chem. A 4 (2016) 4280–4287.

[32] S. Yamakawa, R. Asahi, T. Koyama, Surface segregations in platinum-based alloy nanoparticles, Surf. Sci. 622 (2014) 65–70.

[33] O. Song-Il, J.-M. Yan, H.-L. Wang, Z.-L. Wang, Q. Jiang, High catalytic kinetic performance of amorphous CoPt NPs induced on CeO_x for H_2 generation from hydrous hydrazine, Int. J. Hydrogen. Energy 39 (2014) 3755–3761.

[34] J. Greeley, I.E.L. Stephens, A.S. Bondarenko, T.P. Johansson, H.A. Hansen, T.F. Jaramillo, J. Rossmeisl, I. Chorkendorff, J.K. Nørskov, Alloys of platinum and early transition metals as oxygen reduction electrocatalysts, Nat. Chem. 1 (2009) 552–558.

[35] B. Lim, M. Jiang, P.H.C. Camargo, E.C. Cho, J. Tao, X. Lu, Y. Zhu, Y. Xia, Pd-Pt bimetallic nanodendrites with high activity for oxygen reduction, Science 324 (2009) 1302–1305.

[36] B.A. Kakade, H. Wang, T. Tamaki, H. Ohashi, T. Yamaguchi, Enhanced oxygen reduction reaction by bimetallic CoPt and PdPt nanocrystals, RSC Adv. 3 (2013) 10487–10496.

[37] B.A. Kakade, T. Tamaki, H. Ohashi, T. Yamaguchi, Highly active bimetallic PdPt and CoPt nanocrystals for methanol electro-oxidation, J. Phys. Chem. C 116 (2012) 7464–7470.

[38] A. Serrà, E. Gómez, I.V. Golosovsky, J. Nogués, E. Vallés, Effective ionic-liquid microemulsions based electrodeposition of mesoporous Co-Pt films for methanol oxidation catalysis in alkaline media, J. Mater. Chem. A 4 (2016) 7805–7814.

[39] Q.-S. Chen, S.-G. Sun, Z.-Y. Zhou, Y.-X. Chen, S.-B. Deng, CoPt nanoparticles and their catalytic properties in electrooxidation of CO and CH_3OH studied by in situ FTIRS, Phys. Chem. Chem. Phys. 10 (2008) 3645–3654.

[40] A. Serrà, E. Gómez, M. Montiel, E. Vallés, Effective new method for synthesising Pt and $CoPt_3$ mesoporous nanorods. New catalysts for ethanol electro-oxidation in alkaline medium, RSC Adv. 6 (2016) 47931–47939.

[41] A. Serrà, N. Gimeno, E. Gómez, M. Mora, M. Ll Sagristá, E. Vallés, Magnetic mesoporous nanocarriers for drug delivery with improved therapeutic efficacy, Adv. Funct. Mater 26 (2016) 6601–6611.

[42] L. Vieux-Rochaz, C. Dieppedale, B. Desloges, D. Gamet, C. Barragatti, H. Rostaing, J. Meunier-Carus, Electrodeposition of hard magnetic CoPtP material and integration into magnetic MEMS, J. Micromech. Microeng. 16 (2005) 219–224.

[43] A. Serrà, X. Alcobé, J. Sort, J. Nogués, E. Vallés, Highly efficient electrochemical and chemical hydrogenation of 4-nitrophenol using recyclable narrow mesoporous magnetic CoPt nanowires, J. Mater. Chem. A 4 (2016) 15676–15687.

[44] Y.J. Zhang, Y.T. Yang, Y. Liu, Y.X. Wang, L.L. Yang, M.B. Wei, H.G. Fan, H.J. Zhai, X.Y. Liu, Y.Q. Liu, N.N. Yang, Y.H. Wu, J.H. Yang, A novel approach to the synthesis of CoPt magnetic nanoparticles, J. Phys. D: Appl. Phys. 44 (2011) 295003–295008.

[45] V.K. Gupta, A. Nayak, Cadmium removal and recovery from aqueous solutions by novel adsorbents prepared from orange peel and Fe_2O_3 nanoparticles, Chem. Eng. J. 180 (2012) 81–90.

[46] V.K. Gupta, R. Kumar, A. Nayak, T.A. Saleh, M.A. Barakat, Adsorptive removal of dyes from aqueous solution onto carbon nanotubes: a review, Adv. Colloid Interface Sci. 193–194 (2013) 24–34.

[47] T.A. Saleh, V.K. Gupta, Processing methods, characteristics and adsorption behavior of tire derived carbons: a review, Adv. Colloid Interface Sci. 211 (2014) 93–101.

[48] G. Huang, L. Yang, X. Ma, J. Jiang, S.H. Yu, H.-L. Jiang, Metal-organic framework-templated porous carbon for highly efficient catalysis: the critical role of pyrrolic nitrogen species, Chem. Eur. J. 22 (2016) 3470–3477.

[49] J.-J. Lv, A.-J. Wang, X. Ma, R.-Y. Xiang, J.-R. Chen, J.-J. Feng, One-pot synthesis of porous Pt-Au nanodendrites supported on reduced graphene oxide nanosheets toward catalytic activity reduction of 4-nitrophenol, J. Mater. Chem. A 3 (2015) 290–296.

[50] W. Ye, J. Yu, Y. Zhou, D. Wang, C. Wang, D. Xue, Green synthesis of Pt-Au dendrimer-like nanoparticles supported on polydopamine-functionalized graphene and their high performance toward 4-nitrophenol reduction, Appl. Catal. B: Environ. 181 (2016) 371–378.

[51] Y.-Y. Shen, Y. Sun, L.-N. Zhou, Y.-J. Li, E.S. Yeung, Synthesis of ultrathin PtPdBi nanowire and its enhanced catalytic activity towards p-nitrophenol reduction, J. Matter. Chem. A 2 (2014) 2977–2984.

[52] G. Cui, Z. Sun, H. Li, Z. Liu, Y. Tian, S. Yan, Synthesis and characterization of magnetic elongated hollow mesoporous silica nanocapsules with silver nanoparticles, J. Mater. Chem. A 4 (2016) 1771–1783.

[53] S.K. Ghosh, M. Mandal, S. Kundu, S. Nath, T. Pal, Bimetallic Pt-Ni nanoparticles can catalyse reduction of aromatic nitro compounds by sodium borohydride in aqueous solution, Appl. Catal. A 268 (2004) 61–66.

[54] V.K. Gupta, N. Atar, M.L. Yola, Z. Üstündag, L.A. Uzun, A novel magnetic Fe@Au core-shell nanoparticles anchored graphene oxide recyclable nanocatalysts for the reduction of nitrophenol compounds, Water Res. 48 (2014) 210–217.

[55] M. Zhu, C. Wang, D. Meng, G. Diao, In situ synthesis of silver nanostructures on magnetic Fe_3O_4@C core-shell nanocomposites and their application in catalytic reduction reactions, J. Mater. Chem. A 1 (2013) 2118–2125.

[56] Y. Xie, B. Yan, H. Xu, J. Chen, Q. Liu, Y. Deng, H. Zeng, Highly regenerable Mussel-inspired Fe_3O_4@polydopamine-Ag core-shell microspheres as catalyst and adsorbent for methylene blue removal, ACS Appl. Mater. Interfaces 6 (2014) 8845–8852.

[57] L. Gao, C. Wang, R. Li, Q. Chen, The effect of external magnetic fields on the catalytic activity of Pd nanoparticles in Suzuki cross-coupling reactions, Nanoscale 8 (2016) 8355–8362.

[58] D.M.F. Santos, C.A.C. Sequeira, Sodium borohydride as a fuel for the future, Renew. Sust. Energy Rev. 15 (2011) 3980–4001.

[59] R. Retnamma, A.Q. Novais, C.M. Rangel, Kinetics of hydrolysis of sodium borohydride for hydrogen production in fuel cell applications: a review, Int. J. Hydrogen Energy 36 (2011) 9772–9790.

[60] S. Eugénio, U.B. Demirci, T.M. Silva, M.J. Carmezim, M.F. Montemor, Copper-cobalt foams as active and stable catalysts for hydrogen release by hydrolysis of sodium borohydride, Int. J. Hydrogen. Energy 41 (2016) 8438–8448.

[61] Y. Huang, K. Wang, L. Cui, W. Zhu, A.M. Asiri, X. Sun, Effective hydrolysis of sodium borohydride driven by self-supported cobalt oxide nanorod array for on-demand hydrogen generation, Catal. Commun. 87 (2016) 94–97.

[62] A. Chinnappan, R. Appiah-Ntiamoah, W.-J. Chung, H. Kim, Ionic liquid functionalized graphene oxide decorated with copper oxide nanostructures towards H_2 generation from sodium, Int. J. Hydrogen. Energy 41 (2016) 14491–14497.

[63] S. Gupta, N. Patel, R. Fernandes, D.C. Kothari, A. Mitoello, Mesoporous Co?B nanocatalyst for efficient hydrogen production by hydrolysis of sodium borohydride, Int. J. Hydrogen Energy 38 (2013) 14685–14692.

[64] Y. Wang, P. He, H. Zhou, A novel direct borohydride fuel cell using an acid-alkaline hybrid electrolyte, Energy Environ. Sci. 3 (2010) 1515–1518.

[65] U.B. Demirci, P. Miele, Sodium borohydride versus ammonia borane, in hydrogen storage and direct fuel cell applications, Energy Environ. Sci. 2 (2009) 627–637.

[66] Y. Shang, R. Chen, Semiempirical hydrogen generation model using concentrated sodium borohydride solution, Energy Fuels 20 (2006) 2149–2154.

[67] Y. Liang, P. Wang, H.-B. Dai, Hydrogen bubbles dynamic template preparation of a porous Fe-Co-B/Ni foam catalyst for hydrogen generation from hydrolysis of alkaline sodium borohydride solution, J. Alloy. Compd. 491 (2010) 359–365.

[68] Y. Bai, C. Wu, F. Wu, B. Yi, Carbon-supported platinum catalysts for on-site hydrogen generation from $NaBH_4$ solution, Mater. Lett. 60 (2006) 2236–2239.

[69] C. Xiang, D. Jiang, Z. She, Y. Zou, H. Chu, S. Qiu, H. Zhang, F. Xu, C. Tang, L. Sun, Hydrogen generation by hydrolysis of alkaline sodium borohydride using cobalt-zinc-boron/graphene nanocomposite treated with sodium hydroxide, Int. J. Hydrogen Energy 40 (2015) 4111–4118.

[70] E. Özdemir, Enhanced catalytic activity of Co-B/glassy carbon and Co-B/graphite catalysts for hydrolysis of sodium borohydride, Int. J. Hydrogen Energy 40 (2015) 14045–14051.

[71] Z. Liu, B. Guo, S.H. Chan, E.H. Tang, L. Hong, Pt and Ru dispersed on $LiCoO_2$ for hydrogen generation from sodium borohydride solutions, J. Power Sources 176 (2008) 306–311.

[72] B.H. Liu, Q.A. Li, A highly active Co-B catalyst for hydrogen generation from sodium borohydride hydrolysis, Int. J. Hydrogen Energy 33 (2008) 7385–7391.

[73] S. Ozkar, M. Zahmakiran, Hydrogen generation from hydrolisis of sodium borohydride using Ru(0) nanoclusters as catalyst, J. Alloys Compd. 404-406 (2005) 728–731.

[74] S. Muir, X. Yao, Progress in sodium borohydride as a hydrogen storage material. Development of hydrolysis catalysts and reaction systems, Int. J. Hydrogen Energy 36 (2011) 5983–5997.

[75] N. Patel, R. Fernandes, G. Guella, A. Kale, A. Miotello, B. Patton, C. Zanchetta, Structured and nanoparticle assembled Co-B thin films prepared by pulsed laser deposition: a very efficient catalyst for hydrogen production, J. Phys. Chem. C 112 (2008) 6968–6976.

[76] G. Guella, C. Zanchetta, B. Patton, A. Miotello, New insights on the mechanism of palladium-catalysed hydrolysis of sodium borohydride from ^{11}B NMR measurements, J. Phys. Chem. B 110 (2006) 17024–17033.